An accepted manuscript in Journal of Food Engineering

(DOI: 10.1016/j.jfoodeng.2021.110537, Vol. 300, July 2021, Article No 110357, 8 p.,)

On the Design of Conical Hoppers for Spent Coffee Grounds: Moisture Content and Particle-Size Effects

L. Massaro Sousa[13*], C. G. Schulz[2], R. Condotta[2], and M. C. Ferreira[3].

[1]Process Design and Modeling Division, IFP Energies Nouvelles,
Rond-Point Échangeur de Solaize, 69360 Solaize, France

[2]Chemical Engineering Department, Centro Universitário FEI, Av. Humberto de Alencar Castelo Branco 3972, 09850-901, São Bernardo do Campo, Brazil

[3]Drying Center for Pastes, Suspensions, and Seeds, Chemical Engineering Department, Federal University of São Carlos, P.O. Box 676, 13565-905, São Carlos, Brazil

***** Corresponding author. E-mail address: lucas.massaro-sousa@ifpen.fr (L. Massaro Sousa).

ABSTRACT

Spent coffee ground (SCG) is a food waste with promising potential for reuse in pilot-to-industrial scale processes provided that storage and handling issues are overcome. Here some key bulk and flow properties of SCGs were determined with FT4 rheometer, for powders with different particle-size distribution ($249.1 \leq d_V \leq 583.1$ µm) and moisture content ($2.8\% \leq MC \leq 62.5\%$). These properties were used to evaluate the design of mass-flow silo hoppers following the classical Jenike theory. The SCGs flowability worsened by decreasing d_V and increasing MC, with indexes between $1.09 \leq HR \leq 1.92$ and $2.5 \leq FF \leq 15.0$. The minimum hopper inclination and outlet diameter ranged from 9.9° to 17.1° and 0.40 to 1.00 m. A sensitivity analysis for the hopper design was performed, and a densification equation was coupled to Jenike's method to ease future hopper designs for SCGs with different properties. Ultimately, the results showed that careful consideration must be given to d_V and MC to design effective devices to handle SCGs.

Keywords: biomass, silo, rheometer, powder handling, Jenike.

1 Introduction

Coffee, which is an agricultural product with distinguished taste and aroma, is widely used as an ingredient in the food, pharmaceutical, and cosmetic industries, as well as consumed as a beverage. It is a commodity traditionally produced in emerging countries, such as Brazil, Colombia, and Vietnam, that generated combined revenue of around US$ 11 billion in 2019, which is a major contribution to the countries' trade market (Voora et al., 2019). Over the last decade, global coffee consumption has increased by around 2% annually, reaching almost 10 million tonnes in 2019 (International Coffee Organization, 2019). Owing to the expected growth of the world's population by 25% until 2050, from 7.7 to 9.7 billion people (United Nations, 2019), coffee is likely to play an even bigger role in the coming decades.

Almost 50% of global coffee production is processed for instant coffee making (Mussatto et al., 2011). In the soluble coffee industry, coffee fruit and beans are initially processed into roasted coffee through some separation, drying, milling, and roasting steps, and then soluble coffee powder is obtained from steaming extraction and spray-drying (McNutt and He, 2019; Silva et al., 1998). Spent Coffee Ground (SCG) is the main solid residue generated in this process, at a rate of 2.5 million tons per year. It has a low ash content, and a high heating value similar to that of coal (25 kJ/kg) (Massaro Sousa and Ferreira, 2019a). These characteristics allow using SCG powders to generate renewable energy and steam within the industry, hence contributing to an attractive energy balance in this process.

A general search in the Science Direct database shows that to date, about 1,000 research papers have been published focusing on SCGs, with a significant increase of interest in this topic recently, as the rate of publication has grown from 2 papers/year back in the 90s to about 250 papers in 2020. Overall, these papers focused on reporting physico-chemical

properties for spent coffee grounds (Ballesteros et al., 2014; Massaro Sousa and Ferreira, 2019b; Mussatto et al., 2011; Silva et al., 1998) and on a wide variety of applications, including drying and dewatering (Gómez-de la Cruz et al., 2015; Rocha et al., 2021; Tun et al., 2020), feeding of reactors (Massaro Sousa et al., 2020a, 2020b; Massaro Sousa and Ferreira, 2020a), solid-state fermentation (Murthy and Naidu, 2012), production of biofuels (Al-Hamamre et al., 2012; Kondamudi et al., 2008), extraction of bioactive and antioxidant compounds (Ballesteros et al., 2017; Brazinha et al., 2015; Karmee, 2018), preparing biopolymeric films for food packaging (Coelho et al., 2021; Thiagamani et al., 2017), combustion, gasification, and pyrolysis (Campos-Vega et al., 2015; Kelkar et al., 2015; McNutt and He, 2019; Silva et al., 1998) and so on.

Some key bottlenecks for implementing the previous applications on the pilot and industrial levels are related to the storage and handling of SCGs throughout the units. For instance, it is paramount to design silos with a stable discharge of solids at predictable flow rates, so that they can be used as reliable solid feeders or as intermediary/storage vessels to suppress eventual process instabilities (Barletta et al., 2015; Dai et al., 2012; Ilic et al., 2018; Ramírez-Gómez, 2016). While trial-and-error methods can be used for this design, the results are often disappointing, with the presence of dead zones of solids within the hopper or no solids flow out of the silo. Moreover, in the case of biomass residues such as SCGs, the particle-size distribution, moisture content, and flow attributes vary due to the processing, thus enhancing the difficulties associated with these solids' handling and hopper design.

Recently, some physical and flow properties of dry and moist SCG samples have been determined for the basic understanding of SCGs flowability and compressibility (i.e. repose angle, Hausner ratio, and bulk density) (Massaro Sousa and Ferreira, 2019a, 2019b). However, there is still a gap in knowledge concerning the measurement of flow properties for SCGs with shearing cells, and on using these properties for equipment design.

Therefore, this paper is aimed at understanding the flow pattern of industrial food waste with promising potential for reuse, as well as assisting its storage and handling. First, some key physical and flow properties of SCGs with different particle-size distribution and moisture content were measured with a rheometer. Then, these properties were used to investigate the design of silo hoppers for the effective mass-flow discharge of powders.

2 Material and Methods

2.1 Materials

The SCG samples were prepared by brewing a commercial blend of Arabica and Robusta grains (Três Corações, São Carlos-SP, Brazil). The powders were oven-dried at 105±2 ºC for 24 h and sieved into three base samples named A_{100}, B_{100}, C_{100}. Sample A_{100} has a particle-size distribution between 600 and 500 µm, while the size of sample B_{100} ranges from 500 and 300 µm, and C_{100} lies between 300 and 150 µm.

Additional dry samples were prepared by mixing the coarser samples with the finest one (C_{100}) in a percentage of 10% and 20% in mass, originating samples $A_{90}C_{10}$, $A_{80}C_{20}$, $B_{90}C_{10}$, and $B_{80}C_{20}$. Finally, the base samples were humidified to 20% and 60% on a wet basis by adding water in a glass flask, which was sealed and stored at 4 ºC for 60 h. After every 24 h, the flask was opened and the powder was homogenized to ensure uniform water distribution. The moist samples are designated $A_{100}^{20\%}$, $A_{100}^{60\%}$, $B_{100}^{20\%}$, $B_{100}^{60\%}$, $C_{100}^{20\%}$, and $C_{100}^{60\%}$.

As previously mentioned, a total of seven dry and six moist SCG powders were prepared, aiming at understanding the effect of samples' size and moisture content on SCG flow properties, densification kinetics, and silo hopper design. These samples were selected to cover a wide range of powder properties that are commonly observed in the industrial processing of this biomass waste (Silva et al., 1998).

2.2 Characterization of SCGs properties

Particle-size distribution and mean diameter (De Brouckere diameter - d_V) of the dry samples was measured, in duplicate, by laser diffraction technique using BlueWave model equipment (MicroTrac, Pennsylvania, USA) with air as dispersion media. Particle sizes from 0.01 to 2,800 microns can be accurately measured with this equipment, which covers the size range for the SCGs.

Moisture content (*MC*) of SCG samples was measured with an infrared drying balance model IV-2000 (Gehaka, São Paulo, Brazil) in duplicate. The moisture contents are reported in wet basis.

Bulk density of the samples was evaluated under different normal pressures (*N*) applied to the powder bed in an FT4 rheometer (Freeman Technology, Tewkesbury, UK). First, a known quantity of SCGs is conditioned on the rheometer and based on the volume occupied by the powders, the loose bulk density (ρ_{bl}) is determined. Then, normal pressures of 0.5, 1, 2, 4, 6, 8, 10, 12, and 15 kPa are sequentially applied with a vented piston that allows air to escape from the bed out of the vessel during compression. The reduction of powders volume is measured, and the bulk density at each *N* is obtained. The Hausner ratio (*HR*) is calculated from the ratio of the consolidated bulk density measured at 15 kPa (ρ_{bc}) and $\rho_{bl,}$ as proposed by (Baião et al., 2018).

2.3 Granular shear and wall friction measurements

Powder shear and wall friction measurements were performed in an FT4 rheometer with shear cell accessory: 50 mm of internal diameter and 85 cm³ in volume vessel, a 48 mm shear head diameter and 48 mm diameter disc of stainless steel. The SCG sample was initially homogenized and pre-consolidated within the rheometer by the standard procedure of the equipment, allowing air to escape from the bed out of the vessel in the pre-consolidation stage. After, pre-shear was performed at normal consolidation stresses of 15, 9, 6, and 3 kPa,

followed by a shear step to estimate incipient failure (of the consolidated sample) at 5 different normal stress conditions induced in the powder bed for each level of consolidation, according to ASTM D7891-15 (American Society for Testing Material, 2015). The assays were performed in duplicate for all SCG samples.

From this experiment, the yield locus and effective yield locus are obtained. By plotting the Mohr circles, some flow parameters for the powders are determined, such as cohesion (*c*), angle of internal friction (σ), effective angle of internal friction (δ), unconfined yield strength (*UYS*), major consolidating stress (*MCS*), and flow function (*FF*). The *FF* is obtained from the ratio of *UYS* to *MCS* and is used as a parameter to describe the strength of a bulk solid. Depending on *FF*, the powder flowability is classified as *free-flowing* (*FF*≥10), *easy-flowing* (4≤*FF*<10), *cohesive* (2≤*FF*<4), *very cohesive* (1≤*FF*<2), or *not flowing* (*FF*<1).

Finally, the wall friction angle (ϕ_w) of the powders was estimated by measuring frictional resistance between a metallic disc and SCG samples under consolidation stress from 3 to 15 kPa, in duplicate. The disc is made of stainless steel, which is a material commonly used in the food industry hoppers.

2.4 Conical hopper design

Design of the conical hopper for mass-flow discharge consists of using the measured flow properties with the rheometer for determining the minimum hopper half-angle (θ_m), and minimum hopper outlet size (D_m). In this way, θ_m is calculated according to (Oginni and Fasina, 2018):

$$\theta_m = 90° - 0.5\cos^{-1}[(1-\sin\delta)/2\sin\delta] - \beta \quad (1)$$

$$\beta = [\phi_w + \sin^{-1}(\sin\phi_w/\sin\delta)]/2 \quad (2)$$

After calculating θ_m from Eqs. (1) and (2), it is recommended to adopt a margin of safety for θ_m to allow for differences in the wall surfaces or slight variations in the bulk solid

properties, then the angle should be reduced by 3°. The minimum hopper outlet size is calculated by (Oginni and Fasina, 2018):

$$D_m = H(\theta_m)\sigma_{cr}/(\rho_b g) \quad (3)$$

$$H(\theta_m) = (130 + \theta_m)/65 \quad (4)$$

The critical applied stress (σ_{cr}) represents the limiting value of the unconfined yield strength at which a stable arch can be formed. This value can be obtained from the intersection of the powder flow function (*FF*) with the hopper flow factor line (*ff*) in a graph of the major consolidation stress (x-axis) versus the unconfined yield stress (y-axis). Note that *ff* is a straight-line through the origin with a slope equal to the inverse of *ff* (Fitzpatrick et al., 2004).

Although *ff* can be obtained from the design charts shown in Jenike's famous Bulletin 163 (Jenike, 1964), algebraic expressions derived from these charts are preferred as they can be readily implemented in spreadsheets (Arnold and McLean, 1976; Condotta, 2017; Enstad, 1975). The set of equations are shown below:

$$ff = Y(1 + \sin\delta)H(\theta_m)/[2(X - 1)\sin\theta_m] \quad (5)$$

$$X = 2\sin\delta/(1 - \sin\delta)\,[1 + \sin(2\beta + \theta_m)/\sin\theta_m] \quad (6)$$

$$Y = (A + B)/C \quad (7)$$

$$A = 2[1 - \cos(\beta + \theta_m)]\sin\theta_m \quad (8)$$

$$B = \sin\beta\sin(\beta + \theta_m)\sin(\beta + \theta_m) \quad (9)$$

$$C = (1 - \sin\delta)\sin(\beta + \theta_m)\sin(\beta + \theta_m)\sin(\beta + \theta_m) \quad (10)$$

There are three possible scenarios concerning the intersection of *FF* and *ff* (in the positive x-y quadrant) that might affect determining σ_{cr}, and consequently D_m:

i) if there is an intersection between *FF* and *ff*, σ_{cr} is determined at the y-axis and used to calculate D_m with Eq (3);

ii) if there is no intersection, and *FF* lies above *ff*, the powder does not flow under gravitational discharge or with the proposed hopper wall material;

iii) if there is no intersection, and *FF* lies below *ff*, from the perspective of cohesive arch formation, the powder will flow with any D_m as the applied stress at the hopper outlet overcomes the unconfined yield strength of the arch. In this case, the minimum hopper outlet can be selected either to avoid interlocking effects (usually D_m is 10 to 12 times the diameter of the largest particle (Oginni and Fasina, 2018)) or by other non-standardized criteria based on the handling experience of specific powders or fitted correlations (Chen et al., 2012; Fitzpatrick et al., 2004; Salehi et al., 2019).

3 Results and Discussion

3.1 Physical properties of SCGs

Some key properties of the SCG samples are presented in Table 1, such as the volume mean diameter, moisture content, as well as the loose and consolidated bulk densities measured under pressures of 0 and 15 kPa, respectively. Hausner ratio ($HR=\rho_{bc}/\rho_{bl}$) is an important parameter often used for industrial quality control of pelletizing and feeding operations as it quantifies the flowability and compressibility of powders. Based on this parameter, the lower is the *HR*, the better is the flowability/compressibility of the sample, which generally means a lower likelihood of operational problems related to powders' handling.

It can be observed from Table 1 that the flowability of SCGs worsens as the moisture content increases and as the sample's mean diameter decreases. For example, the flowability of the dry and coarsest sample A_{100} is categorized as *excellent*, whereas the flowability of the finest sample C_{100} is categorized as *passable*. The *HR* of the dry powder mixtures are

intermediary to those of the base samples. Besides, the *HR* increases with the moisture content, then the flowability of sample $A_{100}^{60\%}$ is classified as *very poor*, while $A_{100}^{20\%}$ is *good*, for example. The effect of the moisture content and particle-size distribution on SCGs flowability agree with previous literature results (Massaro Sousa and Ferreira, 2019a).

Table 1. Physical properties of spent coffee ground powders

SCG Sample	d_V (µm)	*MC* (% w.b.)	ρ_{bl} (kg/m³)	ρ_{bc} (kg/m³)	*HR* (-)	Flowability classification
A_{100}	583.1	5.4	386	423	1.09	Excellent
$A_{100}^{20\%}$	-	25.1	368	436	1.18	Good
$A_{100}^{60\%}$	-	58.7	409	609	1.49	Very Poor
B_{100}	442.2	2.8	383	424	1.10	Excellent
$B_{100}^{20\%}$	-	21.4	367	443	1.20	Fair
$B_{100}^{60\%}$	-	62.5	373	610	1.64	Very, Very Poor
C_{100}	249.1	3.1	292	367	1.26	Passable
$C_{100}^{20\%}$	-	21.7	309	412	1.35	Poor
$C_{100}^{60\%}$	-	61.0	299	574	1.92	Very, Very Poor
$A_{90}C_{10}$	549.7	-	405	464	1.14	Good
$A_{80}C_{20}$	516.3	-	381	452	1.19	Fair
$B_{90}C_{10}$	422.9	-	372	424	1.14	Good
$B_{80}C_{20}$	403.6	-	368	428	1.16	Good

3.2 Densification kinetics of SCGs

Evolution of the powder bulk density with the applied pressure is known as the densification curve, with initial and final points as the loose and consolidated bulk densities. The values for ρ_{bl} and ρ_{bc} are presented in Table 1 for all SCG samples. The points and the curvature of the densification curve depend on the bulk material and its properties, such as the particle-size distribution, and moisture content. In this way, assessing the densification of SCGs with different properties is crucial for the effective design and operation of units that handle such biomass powders.

The effect of the particle-size distribution and moisture content on the densification curves of SCGs is shown in Fig. 1. The dry samples exhibit similar densification patterns, with a steep increase in the bulk density prior to N=4 kPa, which represents around 70% of the consolidated bulk density, and a nearly constant bulk density from N=10 kPa onwards, indicating that the maximum bed compaction has been achieved. More specifically, samples A_{100} and B_{100} have similar bulk densities, whereas the curve of the powder mixture $B_{80}C_{20}$ is slightly shifted downwards. Finally, the finest powder C_{100} has the lowest bulk density which might be attributed to enhanced cohesion effects of van der Waals origin (Castellanos, 2005).

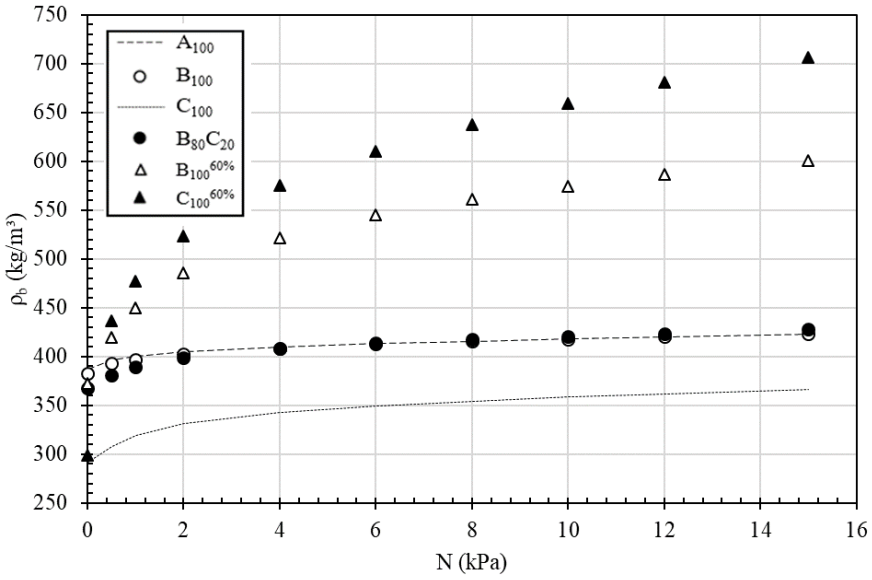

Fig. 1. Bulk density (ρ_b) as a function of the applied normal stress for selected spent coffee ground samples

Adding water to the dry samples increases the bulk density since air voids become partially filled with water, which has a density thousand times greater than the air. For the wet samples, there is a consistent increase in ρ_b with increasing N, and possibly the maximum bed compaction has not been achieved at N=15 kPa. In summary, the densification process is slower for samples with higher cohesion, such as those containing finer particles or higher moisture content. Although only a few SCG samples are shown in Fig. 1, the behavior previously described covers all tested powders.

In a previous study (Massaro Sousa and Ferreira, 2019b), the densification of dry SCGs was assessed by tapping, which means that the powder bed is compacted with the bed weight and not by applying external forces. In general, powder beds 8% denser were achieved with tapping when compared to the applied pressure compaction, which can be attributed to: i) the facilitated rearrangement of particles in the voids promoted by the successive bed vibrations, and ii) limited range of the applied pressure to affect the compaction in the lower portions of the bed. From the practical perspective, these results highlight that for an accurate equipment design some assumptions on the powder densification mechanism should be performed beforehand, i.e., by considering the extent of variation of the bulk density within the equipment as a consequence of the applied normal pressures, and particles rearrangement due to vibration.

In the next section, an analysis is carried out to model the densification curves of SCGs. The aim is to use a single equation to describe the densification process with fitting parameters correlated to SCGs properties. In this way, the bulk density of a certain SCG sample can be readily estimated for a given N.

3.3 Modelling of SCGs densification

In a previous study, the two-parameter equation of Kawakita and Ludde (Eq. 11) (Kawakita and Lüdde, 1971) accurately predicted the densification curves of dry SCGs submitted to tapping. The parameters a and b of the equation could be correlated with the physical properties of the samples, such as the mean diameter and HR (Massaro Sousa and Ferreira, 2019b). Here, Eq. (11) is tested for predicting the densification behavior of dry and wet SCGs submitted to normal pressures. Since the relative density (D) is the ratio of bulk to solid density (ρ_s=1,315 kg/m³ for SCGs (Massaro Sousa and Ferreira, 2019a), the bulk density as a function of N can be explicitly calculated by Eq. (12).

$$(D - D_{bl})/D = abN/(bN + 1) \quad (11)$$

$$\rho_b = \rho_{bl}/[1 - abN/(bN + 1)] \quad (12)$$

The parameters *a* and *b* are shown in Fig. 2 as a function of the *HR* of the samples. From Fig. 2, both parameters in Eq. (11) increase as *HR* rises. These findings are in line with expectations since high *HR* indicates that powder bulk density changes significantly throughout compaction, then high values for *a* and *b* are necessary to describe the steeper variation on the kinetic curves of these powders.

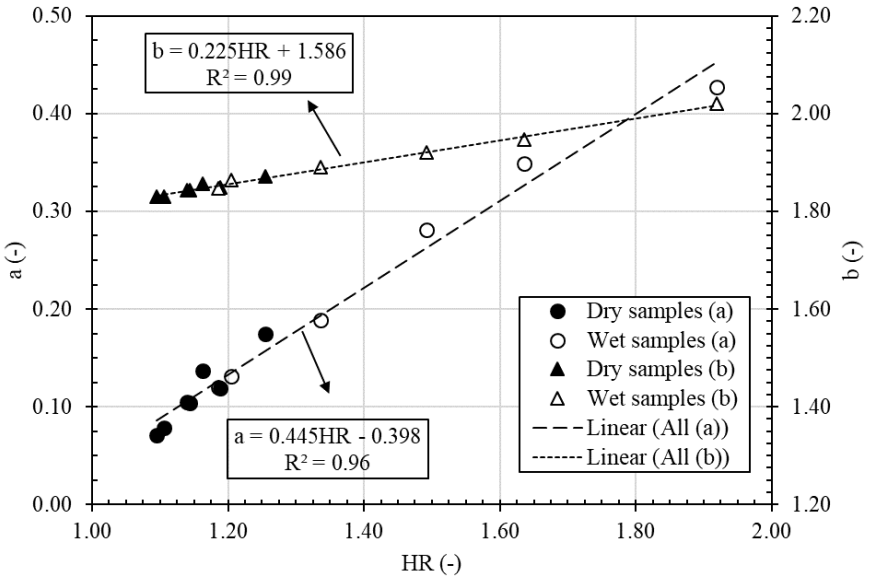

Fig. 2. Parameters *a* and *b* as a function of the samples' Hausner ratio (*HR)*

Linear equations fitted the relationship between the parameters and *HR* accordingly with regression coefficients of 0.99 and 0.96 for Eqs. (13) and (14), respectively. Also, the data are randomly distributed around the lines of the fittings, which is evidence of non-biased fittings.

$$a = 0.445HR - 0.398 \quad (13)$$

$$b = 0.225HR + 1.586 \quad (14)$$

By using Eqs. (12) to (14), it is possible to estimate the bulk density of SCGs for a given *N* provided that both the *HR* and loose bulk density for the sample are known (see

Table 1). Difference between experimental and predicted values of bulk density is on an average of 24% in the range of $0 \leq N \leq 15$ kPa. Nevertheless, we recommend using Eqs. (12) and (13) for predicting ρ_b over $N \geq 2$ kPa as the mean differences lie below 13%. For $N < 2$ kPa the differences reach 40% because the data become more dispersed as the loose bulk condition is approached.

From the above, information on SCGs bulk density can be readily obtained for various normal consolidation pressures, which is useful for equipment design and process control.

3.4 Flow properties of SCGs

In this section, the effect of the particle-size distribution and moisture content on the SCG flow properties measured with the FT4 rheometer is analysed. The flow function and cohesion of the powders are presented in Figures 3a and 3b, respectively, as a function of *N*. Overall, increasing the consolidation pressure leads to lower powder flow functions (Fig. 3a) and higher powder cohesion (Fig. 3b), as particle-particle contacts are enhanced within the rheometer under higher *N*.

Powders with higher *FF* have better flowability; hence, the sample with the finest particles (C_{100}) has the worst flowability among the dry samples. This is due to the higher cohesion of this sample motivated by its greater specific surface area that enhances cohesive forces of van der Waals nature (Castellanos, 2005). Concerning the other dry powders, the flowability of sample A_{100} is worse than sample B_{100} probably due to particle-particle interlocking effects within the rheometer for the coarsest sample, whereas, intermediary *FF* values are observed for the mixtures of coarse and fine particles.

By adding water to the dry SCG samples, cohesive forces of liquid bridge nature become important and powder flowability deteriorates as the moisture content increases. In Fig. 3a and 3b, for example, the wet sample $B_{100}^{60\%}$ exhibits similar *FF* and cohesion than that of sample C_{100}, whereas sample $C_{100}^{60\%}$ has the worst flowability among all SCG samples

due to a combined effect of liquid bridges and van der Wall interactions, since smaller particles saturate its surface at reduced moisture content.

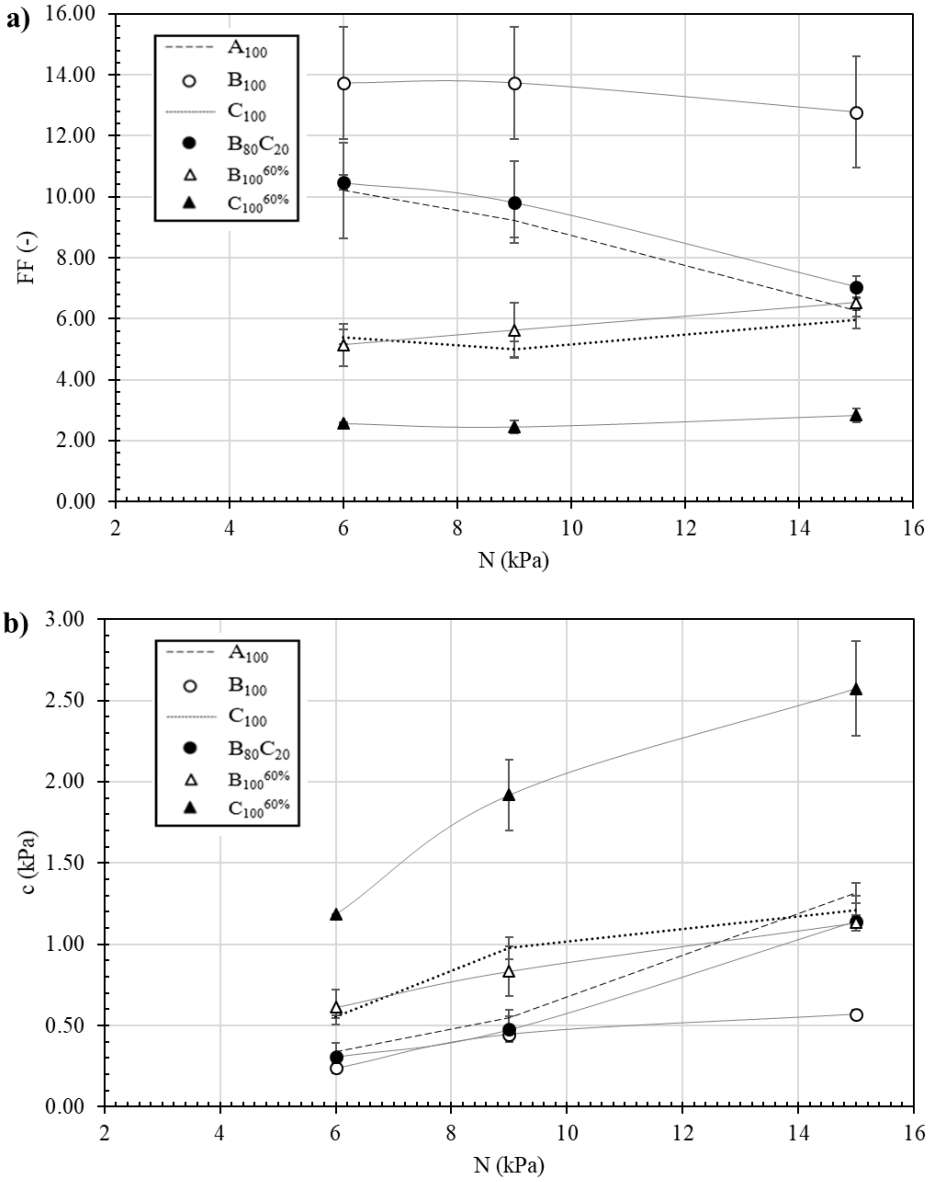

Fig. 3. Flow properties as a function of the consolidation stress for selected spent coffee ground samples: a) flow function and b) cohesion

The previous conclusions concerning the *FF* and cohesion trends are also valid for the SCG samples not shown in Fig. 3. The mean value of *FF* for all samples is presented in Table 2 along with the standard deviation and flowability classification. Although most of the samples are categorized as *easy-flowing* powders with $10<FF<4$, it is noticeable that *FF*

decreases with increasing moisture content and with decreasing particle mean diameter, leading to a *cohesive* behavior for sample $C_{100}^{60\%}$.

Table 2. Averaged values for SCG properties measured with the rheometer and flowability classification

SCG Sample	δ (°)	ϕ_w (°)	*FF* (-)	Flowability classification
A_{100}	40.3 ± 0.4^{a}	25.0 ± 2.0^{a}	9.0 ± 2.0^{a}	Easy flowing
$A_{100}^{20\%}$	41.8 ± 0.5^{b}	27.5 ± 0.3^{a}	6.3 ± 0.9^{b}	Easy flowing
$A_{100}^{60\%}$	42.5 ± 0.9^{b}	26.0 ± 1.0^{a}	6.0 ± 1.0^{b}	Easy flowing
B_{100}	39.8 ± 0.4^{a}	25.0 ± 3.0^{a}	15.0 ± 4.0^{c}	Free flowing
$B_{100}^{20\%}$	41.0 ± 0.8^{ab}	27.2 ± 0.5^{a}	8.0 ± 2.0^{ab}	Easy flowing
$B_{100}^{60\%}$	43.1 ± 0.9^{b}	27.5 ± 0.6^{a}	5.0 ± 1.0^{b}	Easy flowing
C_{100}	40.0 ± 0.7^{a}	27.0 ± 2.0^{a}	5.3 ± 0.5^{b}	Easy flowing
$C_{100}^{20\%}$	40.9 ± 0.5^{ab}	28.8 ± 0.7^{ab}	5.1 ± 0.3^{b}	Easy flowing
$C_{100}^{60\%}$	48.8 ± 0.9^{c}	30.8 ± 0.9^{b}	2.5 ± 0.2^{d}	Cohesive
$A_{90}C_{10}$	40.9 ± 0.7^{ab}	24.0 ± 3.0^{a}	8.0 ± 2.0^{ab}	Easy flowing
$A_{80}C_{20}$	41.1 ± 0.6^{ab}	25.0 ± 2.0^{a}	6.9 ± 0.8^{ab}	Easy flowing
$B_{90}C_{10}$	40.2 ± 0.4^{a}	26.0 ± 2.0^{a}	8.0 ± 2.0^{ab}	Easy flowing
$B_{80}C_{20}$	39.8 ± 0.5^{a}	25.0 ± 2.0^{a}	9.0 ± 2.0^{a}	Easy flowing

* Values with different letters in the same column are significantly different at the 0.05 significance level

The average values for the effective angle of internal friction (δ) and wall friction angle (ϕ_w) are presented in Table 2 along with their standard deviation, measured between N=3 and 15 kPa. Similar to the cohesion and *FF*, both angles vary when N changes from 3 to 15 kPa: while δ exhibits a slight increase as N rises, ϕ_w decreases with increasing N. Besides, δ and ϕ_w increases as the SCGs flowability worsens, i.e., with decreasing particle size and increasing moisture content. These trends agree with results from the literature (Marinelli and Carson, 1992).

In practice, a minor worsening of powder flow attributes may compromise the operation of various types of industrial equipment, such as those for the feeding and storing of solids.

Some evidence of the effect of powder flowability on the solid feeder's performance has been previously assessed in handling dry and moist SCGs to reactors with L-valve and spouted bed feeding devices (Massaro Sousa and Ferreira, 2020a, 2020b). The results of *HR* and *FF* showed in Table 1 and Table 2 indicate that both indices are sensitive to the SCG size and moisture content; hence they might be useful for process monitoring and control.

In the next section, the design of silo hoppers is addressed aiming at an effective mass-flow discharge of SCGs with different properties. Apart from the bulk density (Sections 3.2 and 3.3), the effective angle of internal friction (δ) and wall friction angle (ϕ_w) shown in Table 2 are the properties used for the design of hoppers according to the classical Jenike theory.

3.5 Hopper design for SCGs

In the design of conical hoppers for mass-flow discharge, the minimum hopper angle (θ_m) and the minimum outlet diameter (D_m) are determined based on the powder flow properties. By using the set of Eqs. (1) to (10) and the values of δ and ϕ_w (Table 2), it is possible to obtain θ_m and the hopper flow factor (*ff*) for each SCG sample as shown in Table 3.

The results of θ_m are in line with expectations, and the general trend is that the worse the samples' flow properties are, the greater is the hopper inclination to achieve a mass-flow discharge of SCGs. For example, more inclined hoppers (lower θ_m) are required to make sample C_{100} flow compared to those required for coarser samples A_{100} and B_{100}; Moreover, increasing the moisture content of sample C_{100} from a dry powder to around 60% drops θ_m in almost 30%, from 14.1 to 9.9°. The *ff* is a function of the hopper design and its trend followed the θ_m behavior, as shown in Table 3, with lower values of *ff* as the sample flow attributes worsen.

A common rule of thumb used to achieve mass-flow discharge with powders of unknown flow properties consists of using θ_m= 20°, however, it would not be appropriate to

handle the SCG samples analysed, which highlights the impact of the findings of this study. In real operations, it is likely that funnel discharge or no-flow of SCGs occur with θ_m= 20°; hence, compromising process stability, performance, automation, and safety.

Table 3. Results of the silo design for dry and wet spent coffee ground samples

SCG Sample	θ_m (°)	*ff* (-)	σ_{cr} (Pa)	D_m (m)	D^* (m)
A_{100}	17.0	1.43	-1266	-	0.02
$A_{100}^{20\%}$	13.6	1.38	-871	-	0.02
$A_{100}^{60\%}$	15.7	1.37	992	0.57	-
B_{100}	17.0	1.45	-920	-	0.02
$B_{100}^{20\%}$	13.9	1.40	-1490	-	0.02
$B_{100}^{60\%}$	13.7	1.35	1351	0.83	-
C_{100}	14.1	1.42	509	0.40	-
$C_{100}^{20\%}$	11.6	1.39	-271	-	0.59
$C_{100}^{60\%}$	9.9	1.23	1333	1.00	-
$A_{90}C_{10}$	18.4	1.43	-718	-	0.06
$A_{80}C_{20}$	17.1	1.41	-715	-	0.10
$B_{90}C_{10}$	15.6	1.43	-1024	-	0.06
$B_{80}C_{20}$	17.0	1.45	-683	-	0.10

Additionally to the cone angle limitation, for sample C_{100} and the ones with 60% of moisture content, a minimum hopper diameter (D_m) is required to prevent the formation of cohesive arches (see case iii, Section 2.4). As shown in Table 3, D_m increases as the particle size decreases, thus sample $C_{100}^{60\%}$ has the highest D_m followed by $B_{100}^{60\%}$ and $A_{100}^{60\%}$.

For the other SCG samples, the intersection between *ff* and *FF* is classified as case ii (Section 2.4), which means that the powders might flow for any outlet diameter according to Jenike's theory because the hopper wall inclination is enough to break up cohesive arches. Therefore, in these cases, the outlet diameter is usually set to avoid interlocking effects, with D^* equal to 12 times the size of the largest particle. Nevertheless, since even the bigger SCG

sample diameter is smaller than 1 mm, the range for D^* would be 0.66-0.44 cm, which is far from reasonable for industrial operations.

In the literature, there are some examples of D_m that were proposed based on the author's handling experience for specific powders rather than with the previous rule of thumb. In this way, a more conservative design for the outlet diameter of some SCG samples, denoted by the symbol D^* in Table 3, might be based on the following premises:

- D^* of sample $C_{100}^{20\%}$ was obtained by linearly interpolating D_m of samples C_{100} and $C_{100}^{60\%}$ concerning the moisture content reported in Table 1;
- Sample B_{100} and one with 30% of moisture content presented stable discharge from silo hoppers of θ_m=30° and D_m=2.1 cm in a previous study (Massaro Sousa and Ferreira, 2020a). Therefore, D^*=2.1 cm was set for samples B_{100}, and $B_{100}^{20\%}$, however, without assertiveness on whether it is a mass- or funnel-flow discharge. As samples A_{100} and $A_{100}^{20\%}$ have similar flow properties than B_{100}, and $B_{100}^{20\%}$, the same D^* was set to these powders.
- D^* of samples $A_{90}C_{10}$, $A_{80}C_{20}$, $B_{90}C_{10}$, and $B_{80}C_{20}$ were obtained based on a weighted average of D_m of samples A_{100} and C_{100} with respect to the fraction of fines in the mixture.

It should be noted that the reported values for D_m vary ± 0.5% and 1.3% by considering the upper and lower limits of the averaged δ and ϕ_w shown in Table 2, respectively. Meanwhile, θ_m vary 0.5% and 9.0% in the same range of variation for δ and ϕ_w. In the next section, the effect of variations on the main parameters used for determining θ_m and D_m are discussed in detail.

3.6 Sensitivity of hopper design for SCGs

The particle-size distribution and moisture level of spent coffee grounds are not controlled in industrial processes due to its residue-based nature. Thus, there is some

variability on samples' flow and bulk properties, as illustrated in the previous sections, which ultimately might affect the design of hoppers for the mass-flow discharge of these biomass powders.

The effect of δ and ϕ_w on the minimum hopper half-angle and hopper flow factor is depicted in Fig. 4a and 4b, respectively. Overall, θ_m is mainly affected by variations in ϕ_w, and steeper hoppers are required to achieve mass flow discharge of powders with higher ϕ_w. On the other hand, *ff* is mostly affected by δ following an inversely proportional linear relationship. For intersections between *ff* and *FF* classified as the case i (Section 2.4), it means that samples with lower values of δ have greater *ff* and $\sigma_{cr,}$ which leads to wider outlet diameters required to achieve mass-flow discharge of solids from the hopper.

Finally, in Fig. 4c it is shown that both the bulk density and σ_{cr} (or implicitly *FF*) play a major role in the calculated outlet hopper diameter. For example, for intersections between *ff* and *FF* classified as case i (Section 2.4), the lower is the *FF* (i.e. powders with worse flowability) the higher is σ_{cr}; hence, wider hopper diameters are required to achieve the mass-flow discharge of SCGs. Furthermore, higher is the bulk density at the cone outlet, the smaller is the required hopper diameter size for the gravity-driven, mass-flow discharge of solids. As shown in Section 3.3, Eqs. (12) to (14) provide a reliable estimation of the bulk density for dry and wet SCGs under different normal pressures; hence, these equations coupled to Jenike's method are useful to meet specific requirements for silos with SCGs in the pilot and industrial-scale plants, as well for improving automation and process monitoring.

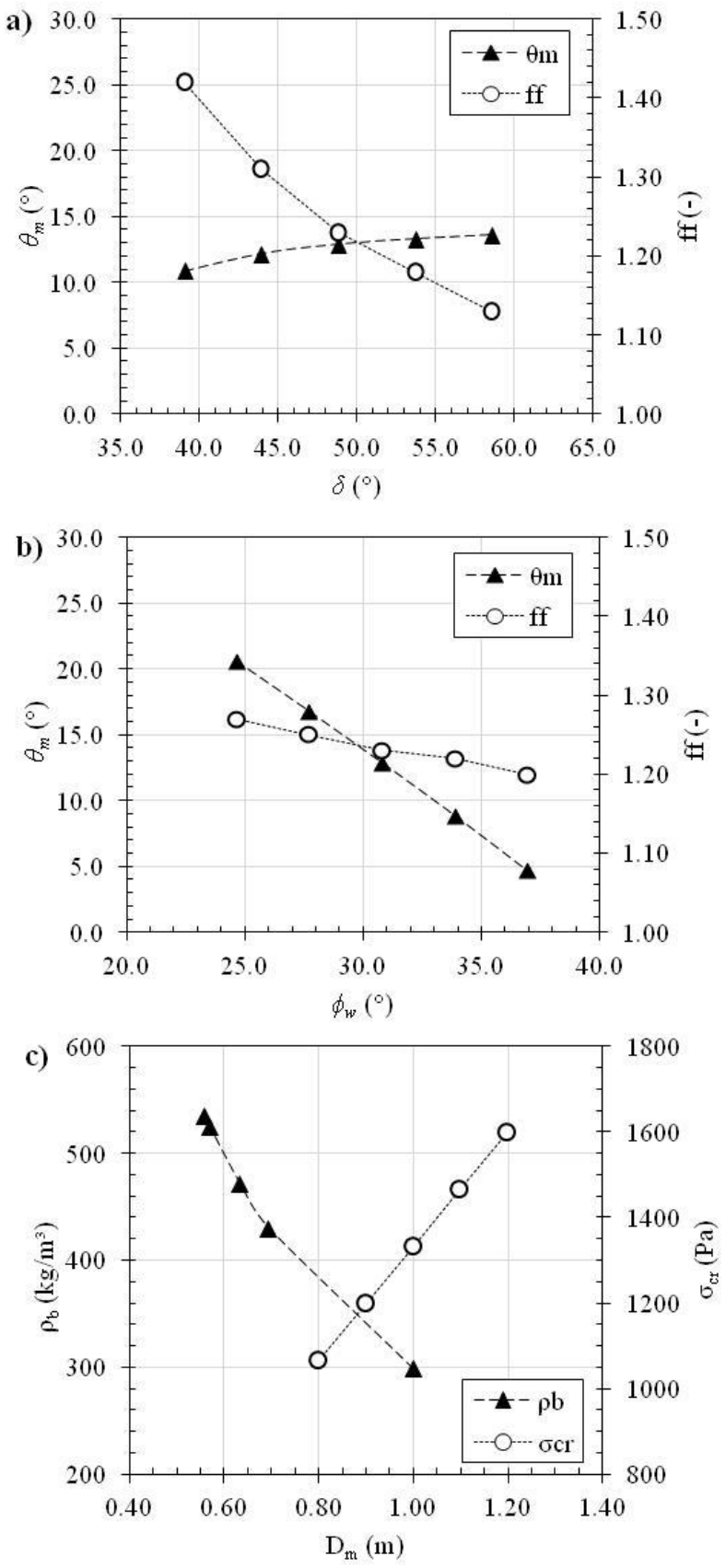

Fig. 4. Hopper flow factor (*ff*) and hopper half-angle (θ_m) with respect to variations in a) δ and b) ϕ_w, as well as hopper diameter response to changes in c) ρ_b and σ_{cr}

4 Conclusions

This study corroborates that the mean particle diameter and moisture content play an important role in both bulk properties and flow attributes of SCGs, hence impacting the design of silo hoppers for the effective mass-flow discharge of powders. Flowability of SCGs deteriorated with decreasing particle-size and increasing moisture content.

From the practical point of view, silo hoppers with inclination and outlet diameter between 9.9° to 17.1°, and 0.40 to 1.00 m are sufficient to handle most SCG powders. It is also shown that a densification equation can be coupled to Jenike's method, which might facilitate the further design of silo hoppers for SCGs with different properties.

The findings are valuable for solid-waste researchers and practitioners aiming at the effective handling of SCGs. Future research could address the design of hoppers for other relevant food wastes with different material properties, as well as numerical simulations to investigate particle segregation effects on the hopper discharge for waste biomass powders.

Acknowledgements

The authors would like to thank the São Paulo Research Foundation (2016/25946-2 and 2018/11031-8), CNPq (114863/2018-0) and CAPES (Finance code 001) for financial support, as well as Prof. Dr. Diego Barletta (Università Degli Studi di Salerno/ Italy) for the valuable discussions concerning the hopper design method.

Nomenclature

A	Parameter calculated as per Eq. (8) (-)
a	Empirical parameter in Eq. (11) (-)
B	Parameter calculated as per Eq. (9) (-)
b	Empirical parameter in Eq. (11) (-)
C	Parameter calculated as per Eq. (10) (-)
c	Cohesion (kPa)
D	Relative density (-)
D_{bl}	Relative density at loose bulk condition (-)
D_m	Jenike's minimum hopper outlet size (m)
D^*	Empirical minimum hopper outlet size (m)

d_V	De Brouckere mean diameter (μm)
ff	Hopper flow factor line (-)
FF	Flow function (-)
g	Gravity acceleration ($m.s^{-2}$)
$H(\theta_m)$	Parameter calculated as per Eq. (4) (-)
HR	Hausner ratio (-)
MC	Moisture content (% w.b.)
MCS	Major consolidating stress (kPa)
N	Consolidating pressure (kPa)
UYS	Unconfined yield strength (kPa)
X	Parameter calculated as per Eq. (6) (-)
Y	Parameter calculated as per Eq. (7) (-)

Greek symbols

β	Parameter calculated as per Eq. (2) (°)
ρ_b	Bulk density ($kg.m^{-3}$)
ρ_{bl}	Loose bulk density ($kg.m^{-3}$)
ρ_{bc}	Consolidated bulk density ($kg.m^{-3}$)
ρ_s	Solid density ($kg.m^{-3}$)
ϕ_w	Wall friction angle (°)
θ_m	Jenike's minimum hopper half angle (°)
σ	Angle of internal friction (º)
σ_{cr}	Critical applied stress (Pa)
δ	Effective angle of internal friction (°)

References

Al-Hamamre, Z., Foerster, S., Hartmann, F., Kröger, M., Kaltschmitt, M., 2012. Oil extracted from spent coffee grounds as a renewable source for fatty acid methyl ester manufacturing. Fuel 96, 70–76.

American Society for Testing Material, 2015. Standard test method for shear testing of powders using the freeman technology FT4 powder rheometer shear cell. ASTM D7891-15.

Arnold, P.C., McLean, A.G., 1976. Improved analytical flowfactors for mass-flow hoppers. Powder Technol. 15, 279–281.

Baião, D.B., Machado, C.S., Condotta, R., 2018. Bidisperse mixtures of sand: effects of granulometry on its packing and flowability. J. Eng. Exact Sci. 04, 117–126.

Ballesteros, L.F., Ramirez, M.J., Orrego, C.E., Teixeira, J.A., Mussatto, S.I., 2017. Optimization of autohydrolysis conditions to extract antioxidant phenolic compounds from spent coffee grounds. J. Food Eng. 199, 1–8.

Ballesteros, L.F., Teixeira, J.A., Mussatto, S.I., 2014. Chemical, functional, and structural properties of spent coffee grounds and coffee silverskin. Food Bioprocess Technol. 7, 3493–3503.

Barletta, D., Berry, R.J., Larsson, S.H., Lestander, T.A., Poletto, M., Ramírez-Gómez, Á., 2015. Assessment on bulk solids best practice techniques for flow characterization and storage/handling equipment design for biomass materials of different classes. Fuel Process. Technol. 138, 540–554.

Brazinha, C., Cadima, M., Crespo, J.G., 2015. Valorisation of spent coffee through membrane processing. J. Food Eng. 149, 123–130.

Campos-Vega, R., Loarca-Piña, G., Vergara-Castañeda, H.A., Oomah, B.D., 2015. Spent coffee grounds: a review on current research and future prospects. Trends Food Sci. Technol. 45, 24–36.

Castellanos, A., 2005. The relationship between attractive interparticle forces and bulk behaviour in dry and uncharged fine powders. Adv. Phys. 54, 263–376.

Chen, P., Yuan, Z., Shen, X., Zhang, Y., 2012. Flow properties of three fuel powders. Particuology 10, 438–443.

Coelho, G.O., Batista, M.J.A., Ávila, A.F., Franca, A.S., Oliveira, L.S., 2021. Development and characterization of biopolymeric films of galactomannans recovered from spent coffee grounds. J. Food Eng. 289, 110083.

Condotta, R., 2017. Coulabilite des poudres cohesives. Press. Académiques Francoph.

Dai, J., Cui, H., Grace, J.R., 2012. Biomass feeding for thermochemical reactors. Prog. Energy Combust. Sci. 38, 716–736.

448 Enstad, G., 1975. On the theory of arching in mass flow hoppers. Chem. Eng. Sci. 30, 1273–
449 1283.
450 Fitzpatrick, J.J., Barringer, S.A., Iqbal, T., 2004. Flow property measurement of food powders
451 and sensitivity of Jenike's hopper design methodology to the measured values. J. Food
452 Eng. 61, 399–405.
453 Gómez-de la Cruz, F.J., Cruz-Peragón, F., Casanova-Peláez, P.J., Palomar-Carnicero, J.M.,
454 2015. A vital stage in the large-scale production of biofuels from spent coffee grounds:
455 The drying kinetics. Fuel Process. Technol. 130, 188–196.
456 Ilic, D., Williams, K., Farnish, R., Webb, E., Liu, G., 2018. On the challenges facing the
457 handling of solid biomass feedstocks. Biofuels, Bioprod. Biorefining 12, 187–202.
458 International Coffee Organization, 2019. World Coffee Consumption [WWW Document].
459 URL http://www.ico.org/ (accessed 11.15.19).
460 Jenike, A.W., 1964. Storage and flow of solids. Bull. 163.
461 Karmee, S.K., 2018. A spent coffee grounds based biorefinery for the production of biofuels,
462 biopolymers, antioxidants and biocomposites. Waste Manag. 72, 240–254.
463 Kawakita, K., Lüdde, K.H., 1971. Some considerations on powder compression equations.
464 Powder Technol. 4, 61–68.
465 Kelkar, S., Saffron, C.M., Chai, L., Bovee, J., Stuecken, T.R., Garedew, M., Li, Z., Kriegel,
466 R.M., 2015. Pyrolysis of spent coffee grounds using a screw-conveyor reactor. Fuel
467 Process. Technol. 137, 170–178.
468 Kondamudi, N., Mohapatra, S.K., Misra, M., 2008. Spent coffee grounds as a versatile source
469 of green energy. J. Agric. Food Chem. 56, 11757–11760.
470 Marinelli, J., Carson, J.W., 1992. Solve solids flow problems in bins, hoppers, and feeders.
471 Chem. Eng. Prog. 88, 22–28.
472 Massaro Sousa, L., Ferreira, M.C., 2020a. Analysis of the Performance of an L-Valve

Feeding Spent Coffee Ground Powders into a Circulating Fluidized Bed. Powder Technol. 362, 759–769.

Massaro Sousa, L., Ferreira, M.C., 2020b. On the Performance of a Spouted Bed type Device for Feeding Spent Coffee Grounds to a Circulating Fluidized Bed Reactor. Chem. Eng. Res. Des. 160, 31–38.

Massaro Sousa, L., Ferreira, M.C., 2019a. Spent coffee grounds as a renewable source of energy: An analysis of bulk powder flowability. Particuology 43, 92–100.

Massaro Sousa, L., Ferreira, M.C., 2019b. Densification behavior of dry spent coffee ground powders: Experimental analysis and predictive methods. Powder Technol. 357, 149–157.

Massaro Sousa, L., Ferreira, M.C., Hou, Q.F., Yu, A.B., 2020a. Feeding Spent Coffee Ground Powders with a Non-Mechanical L-valve: Experimental Analysis and TFM Simulation. Powder Technol. 360, 1055–1066.

Massaro Sousa, L., Ferreira, M.C., Hou, Q.F., Yu, A.B., 2020b. Feeding Spent Coffee Grounds into Reactors: TFM Simulation of a Non-Mechanical Spouted Bed Type Feeder. Waste Manag. 109, 161–170.

McNutt, J., He, Q., 2019. Spent coffee grounds: A review on current utilization. J. Ind. Eng. Chem. 71, 78–88.

Murthy, P.S., Naidu, M.M., 2012. Production and application of xylanase from Penicillium sp. utilizing coffee by-Products. Food Bioprocess Technol. 5, 657–664.

Mussatto, S.I., Machado, E.M.S., Martins, S., Teixeira, J.A., 2011. Production, composition, and application of coffee and its industrial residues. Food Bioprocess Technol. 4, 661–672.

Oginni, O., Fasina, O., 2018. Theoretical estimation of silo design parameters for fractionated loblolly pine grinds – Moisture content and particle size effects. Ind. Crops Prod. 123, 379–385.

Ramírez-Gómez, A., 2016. Research needs on biomass characterization to prevent handling problems and hazards in industry. Part. Sci. Technol. 34, 432–441.

Rocha, T.A.F., Ferreira, M.C., Freire, J.T., 2021. Processing spent coffee ground powders for renewable energy generation: Mechanical dewatering and thermal drying. Process Saf. Environ. Prot. 146, 300–311.

Salehi, H., Poletto, M., Barletta, D., Larsson, S.H., 2019. Predicting the silo discharge behavior of wood chips - A choice of method. Biomass and Bioenergy 120, 211–218.

Silva, M.A., Nebra, S.A., Machado Silva, M.J., Sanchez, C.G., 1998. The use of biomass residues in the Brazilian soluble coffee industry. Biomass and Bioenergy 14, 457–467.

Thiagamani, S.M.K., Nagarajan, R., Jawaid, M., Anumakonda, V., Siengchin, S., 2017. Utilization of chemically treated municipal solid waste (spent coffee bean powder) as reinforcement in cellulose matrix for packaging applications. Waste Manag. 69, 445–454.

Tun, M.M., Raclavská, H., Juchelková, D., Růžičková, J., Šafář, M., Štrbová, K., Gikas, P., 2020. Spent coffee ground as renewable energy source: Evaluation of the drying processes. J. Environ. Manage. 275, 111204.

United Nations, 2019. World population prospects: Highlights [WWW Document]. Dep. Econ. Soc. Aff. Popul. Div. URL www.ncbi.nlm.nih.gov/pubmed/12283219

Voora, V., Bermúdez, S., Larrea, C., 2019. Sustainable Commodities Marketplace Series - Global Market Report: Coffee [WWW Document]. URL https://www.iisd.org/publications/global-market-report-coffee